Technical University of Denmark

DTU

Correlated thermal motion of two liquid Pb inclusions attached to a fixed dislocation in an Al matrix
Paper

Prokofjev, Sergei I.; Johnson, Erik

Link back to DTU Orbit

DTU Library
Technical Information Center of Denmark

PAPER • OPEN ACCESS

Correlated thermal motion of two liquid Pb inclusions attached to a fixed dislocation in an Al matrix

View the article online for updates and enhancements.

Journal of Physics Communications

CrossMark

Correlated thermal motion of two liquid Pb inclusions attached to a fixed dislocation in an Al matrix

Sergei I Prokofjev[1] and Erik Johnson[2,3]

1   Institute of Solid State Physics of the Russian Academy of Sciences, Academician Ossipyan str. 2, Chernogolovka, Moscow District, 142432, Russia
2   Center for Quantum Devices, Copenhagen, Niels Bohr Institute, University of Copenhagen, Universitetsparken 5, DK-2100 Copenhagen, Denmark
3   Department of Wind Energy, Technical University of Denmark, DTU Risø Campus, Frederiksborgvej 399, DK-4000 Roskilde, Denmark

E-mail: prokof@issp.ac.ru

Abstract

Thermal motion of two liquid lead inclusions attached to the same fixed dislocation in an Al-0.65 at% Pb alloy is studied *in situ* at 447 °C using transmission electron microscopy. Observations of their motion is recorded on video and analyzed frame by frame. Random oscillatory motion of the inclusions on the dislocation line occurs as a result of their mutual repulsion and their repulsion from the fixed ends of the dislocation caused by the dislocation line tension. The oscillations of the inclusions can be considered as correlated thermal motion in coupled potential wells. The effective potentials, in which the inclusions move, and the effective potential of their interactions are evaluated. It is found that the spatial correlations of the positions of the inclusions on the dislocation depend strongly on the interaction potential. The observed correlations of the positions of the inclusions suggest that they move along their averaged trajectories in a synchronous-like manner.

1. Introduction

Transmission electron microscopy (TEM) observations show that small liquid inclusions of a second phase in a crystalline matrix can carry out significant thermal motion at elevated temperature. Whilst free inclusions in the matrix can exhibit 'traditional' 3D random walk [1–3], one or several inclusions attached to a fixed dislocation exhibit oscillations around the dislocations line [3–7]. This behavior can be explained by elastic interactions between the inclusions and the dislocation [3, 5, 8]. From thermal motion data obtained in *in situ* TEM experiments the diffusion coefficients of He bubbles [9] and liquid Pb inclusions [3–5, 10] attached to fixed dislocations in Al-based alloys were determined. It was shown that for inclusions of a given size the diffusivities of free inclusions and inclusions attached to dislocations were comparable [3]. Investigation of the diffusion coefficients as a function of inclusion size of liquid Pb inclusions attached to fixed dislocations in Al indicates that the diffusivity of the inclusions is controlled by step formation on {111}Al/Pb faces of the inclusions in a wide temperature range [10] (Atomically flat {111} faces on the surface of small liquid Pb inclusions in a crystalline Al matrix are retained at temperature much higher than melting temperature of the inclusions [11, 12].) in good agreement with the model proposed by Willertz and Shewmon [13]. However, the size dependence of the inclusion diffusivity at higher temperatures, when liquid Pb inclusions are rounded, suggests according to [14] that diffusion of the inclusions is probably mediated by atomic diffusion along the Al/Pb interfaces [3] or even by atomic bulk diffusion through the matrix [7].

Interactions of second phase inclusions with dislocations have been investigated in numerous studies since inclusions often control the mechanical properties of multiphase alloys [15–17]. However, the inclusions usually act as immobile obstacles for dislocations or they are dragged along passively with the moving dislocations [18, 19]. The elastic interaction between inclusions undergoing thermal motion while attached to a fixed

Figure 1. (a) TEM micrograph (single video frame) of the two inclusions attached to the dislocation segment (out of contrast), whose ends are fixed at two inclusions of much larger sizes. (b) Trajectories of the thermal motion of the inclusions (shifted vertically to avoid overlap). After [5].
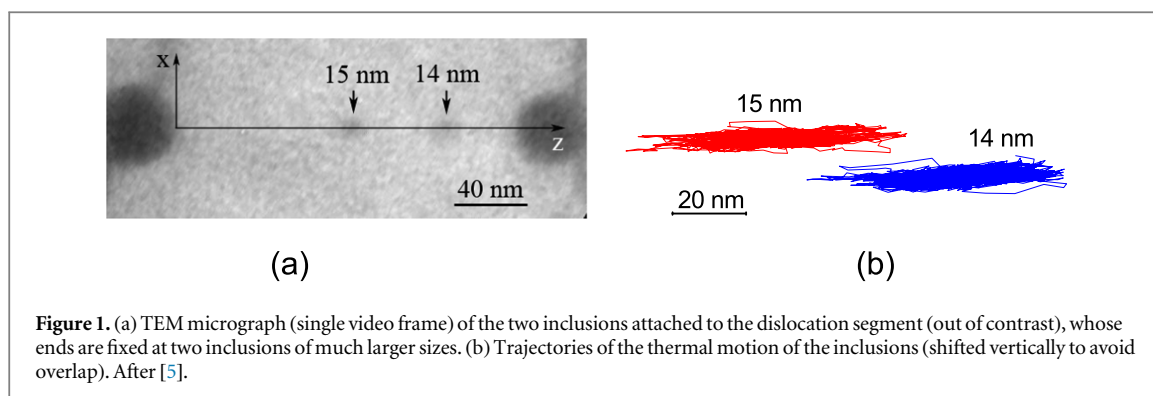
dislocation is usually not considered. As a result, many features of the kinetic behavior of inclusions attached to dislocations remain almost unexplored, although the problem is of basic interest. In addition, thermal motion of inclusions attached to dislocations can contribute to the mechanical properties [20] of multiphase alloys at elevated temperature as a large fraction of inclusions is usually attached to dislocations.

Earlier, we had reported the study of thermal motion of two nano-sized liquid Pb inclusions attached to a fixed dislocation in an Al matrix at 447 °C using *in situ* TEM, where the indication was found the inclusions interacted with each other [6]. In our later paper [8] the shape of the potential of the interaction of these inclusions was evaluated using the experimental data obtained in [6]. The present paper considers comprehensively thermal motion of the same two inclusions attached to the dislocation. Features of their thermal motion due to the dislocation elasticity are considered in detail, and the strong evidence of spatially correlated thermal motion of the inclusions attached to a fixed dislocation is obtained that is the first such observation. Necessary experimental details based on [5, 6] are given in section 2. Section 3.1 presents shortly the experimental data-set presented originally in [6]. Section 3.2 considers the longitudinal thermal motion of the inclusions and their interaction. The effect of elasticity of fixed dislocation on thermal motion of two inclusions attached is shown in section 4. Transverse thermal motion of the inclusions is considered in section 5. In section 6 spatial correlations in the inclusions thermal motion are characterized, and their manifestations are also presented.

2. Experimental procedure

Thin foils for TEM were prepared from a rapidly solidified melt spun ribbon of an Al(5N)-0.65 at% Pb(6N) alloy quenched from a temperature above the Al–Pb liquid miscibility gap. After a stabilizing anneal at a temperature of 280 °C for 2 h in an Ar atmosphere the equilibrated microstructure of the alloy consisted of Pb-rich nano-sized inclusions embedded in the polycrystalline matrix of almost pure aluminum according to the Al–Pb phase diagram [21].

In situ TEM observations of thermal motion of the inclusions were carried out at a temperature of 447 °C in a 200 kV Philips CM 20 microscope using a single tilt heating stage (Gatan). The accuracy of the sample temperature control was around 1 °C. The estimated error in the absolute temperature determination was around 5 °C.

The observations were recorded on video (25 video frames per second), digitized, and split into individual frames, where the coordinates of the positions (centers) of the inclusions were measured. The total video-sequence contained 2687 digitized images. After correction for sample drift, the inclusion trajectories were measured from their projected positions on each of these images. The inclusion sizes and the dislocation length were measured as well. More experimental details can be found in [5, 6].

3. Results and analysis

3.1. Character of thermal motion of the inclusions

Figure 1(a) shows the two liquid Pb inclusions with rounded shape attached to the same dislocation in the Al matrix at 447 °C. Fragment of video record of their thermal motion is available online at stacks.iop.org/JPCO/1/055001/mmedia as a supporting material[4]. Their average diameters of the inclusions are 15 nm and 14 nm respectively. The dislocation segment fixed at two large inclusions at the ends is out of contrast in this picture.

---

[4] See supplemental material at stacks.iop.org/JPCO/1/055001/mmedia for real-time *in situ* TEM video of thermal motion of the two liquid Pb inclusions on the dislocation.
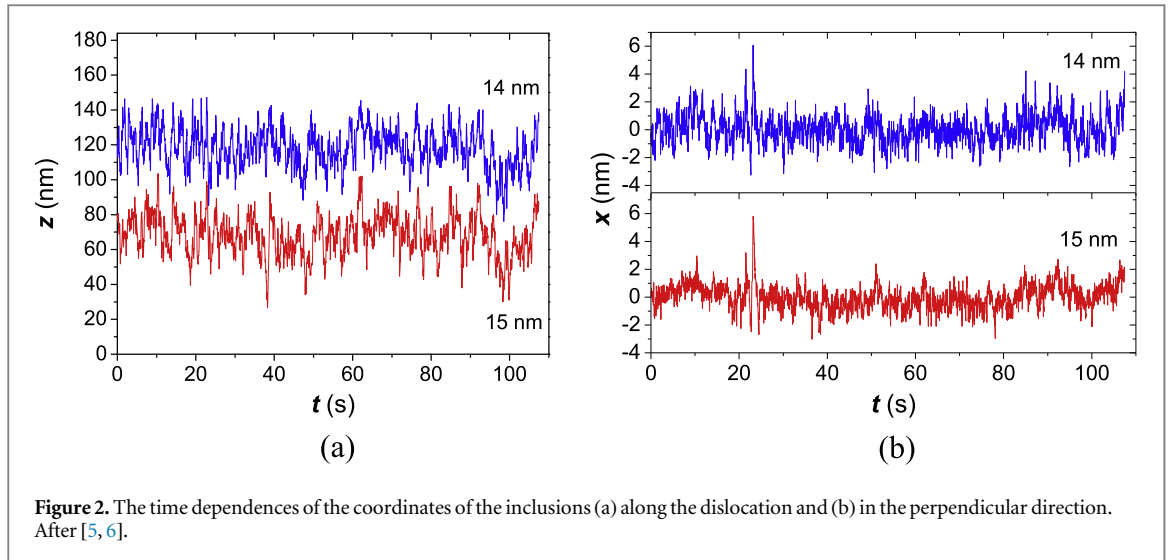
Figure 2. The time dependences of the coordinates of the inclusions (a) along the dislocation and (b) in the perpendicular direction. After [5, 6].
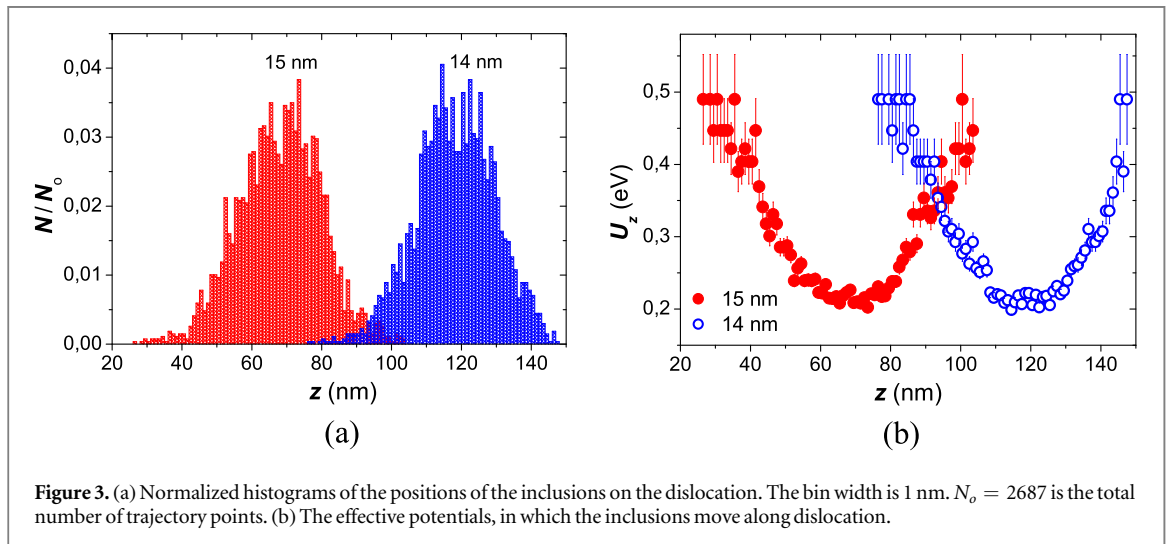
Figure 3. (a) Normalized histograms of the positions of the inclusions on the dislocation. The bin width is 1 nm. $N_o = 2687$ is the total number of trajectory points. (b) The effective potentials, in which the inclusions move along dislocation.

The position of the dislocation line approximately coincides with the z-axis in figure 1(a). The average measured dislocation length is $L = 184$ nm. The z-coordinates of its fixed ends are $z_o = 0$ nm and $z_L = 184$ nm. The trajectories of the thermal motion of the inclusions are shown in figure 1(b). They are elongated because the major component of the movement is along the dislocation line. In the following, the coordinates of the 15 nm and 14 nm inclusions will be referred as (x_1, z_1) and (x_2, z_2), respectively.

The positions of the inclusions along the dislocation line (z-axis) and in the transverse x-direction as functions of time are shown in figures 2(a) and (b), respectively. The graphs show a chaotic-like oscillatory motion of the inclusions.

3.2. Longitudinal thermal motion and interaction of the inclusions

The normalized histograms presenting the probability distributions of the z-positions of the inclusions along the dislocation line have pronounced maxima as shown in figure 3(a). The effective potentials in which the inclusions move, are derived from these histograms using the equation

$$U_z = -kT \ln [N/N_o] \qquad (1)$$

following from the Boltzmann distribution law. Here N is the number of points of the trajectory in the bin of coordinate z with a width of 1 nm, $N_o = 2687$ is the total number of points of trajectory, T is the absolute temperature, and k is the Boltzmann constant. The effective potentials obtained using equation (1) are presented in figure 3(b). Their 'potential well' shapes suggest that the inclusions interact with each other and with the fixed ends of the dislocation. Because of a reference energy level uncertainty, only the depths of the wells, which are about 0.3 eV, have a physical meaning. For comparison, $kT = 0.062$ eV.
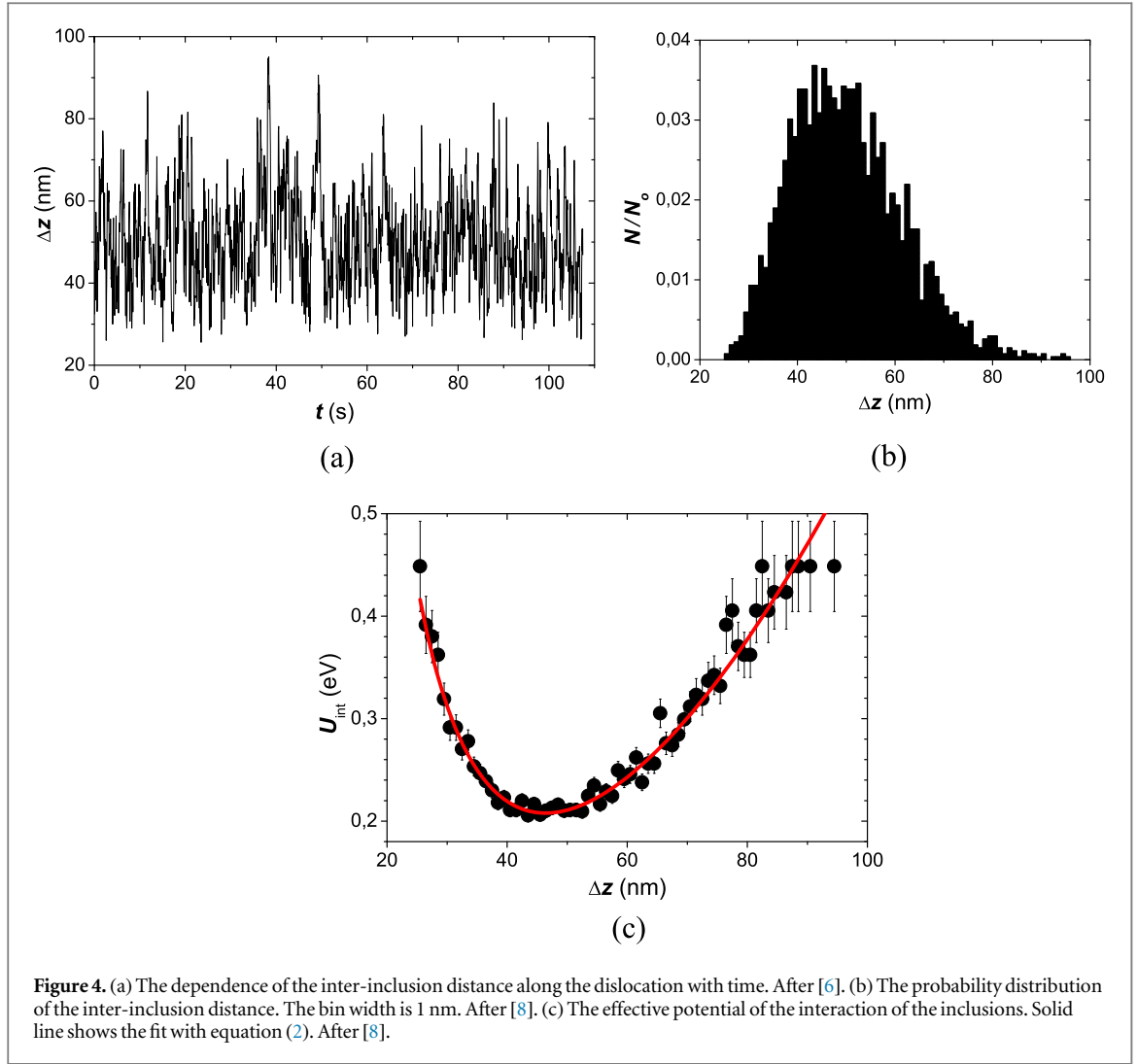
Figure 4. (a) The dependence of the inter-inclusion distance along the dislocation with time. After [6]. (b) The probability distribution of the inter-inclusion distance. The bin width is 1 nm. After [8]. (c) The effective potential of the interaction of the inclusions. Solid line shows the fit with equation (2). After [8].

In order to describe the interaction between the inclusions the inter-inclusion distance along the dislocation $\Delta z = z_2 - z_1$ was determined for each measured time point. The time dependence of Δz demonstrates an apparently chaotic oscillatory behavior, figure 4(a). From the histogram of the separation of the inclusions Δz shown in figure 4(b) the effective potential of the interaction of the inclusions $U_{\mathrm{int}}(\Delta z)$ is obtained, figure 4(c) in the same way as it was done above for the z-movements of the inclusion. It demonstrates mutual repulsion of the inclusions at $\Delta z < \Delta z_{\mathrm{m}}$ and attraction at $\Delta z > \Delta z_{\mathrm{m}}$, where Δz_{m} corresponds to the minimum U_{m} of the interaction potential. Indeed, coalescence of the inclusions was not observed during the entire observation time of more than 10 min [6], although the distributions of the positions of the inclusions on the dislocation partially overlap, figure 3(a). Furthermore, the inclusions did not coalesce with the large inclusions at the fixed ends of the dislocation either. The behavior of the interaction potential is described well by the equation

$$U_{\mathrm{int}}(\Delta z) = \frac{U_{\mathrm{m}}}{2}\left[\left(\frac{\Delta z}{\Delta z_{\mathrm{m}}}\right)^{-2} + \left(\frac{\Delta z}{\Delta z_{\mathrm{m}}}\right)^{2}\right] + U_o. \qquad (2)$$

The powers of 2 and -2, respectively, in the empirical potential were found from a log–log plot of the coordinates giving straight lines with slopes of 2 and -2 of the potential far from the minimum [8]. Then, the analytical shape (2) was found by expressing the coefficients in the equation $A_{\mathrm{rep}}\Delta z^{-2} + A_{\mathrm{att}}\Delta z^2$ through coordinates of the minimum, Δz_{m} and U_{m}. Fit of (2) to the experimental points gives $\Delta z_{\mathrm{m}} = 46.4 \pm 0.2$ nm, $U_{\mathrm{m}} = 0.26 \pm 0.01$ eV and $U_o = -0.05 \pm 0.01$ eV. Here the adjusted parameter U_o is introduced for uncertainty of the energy level.

4. Effect of elasticity of the dislocation on thermal motion of the inclusions

In [3, 5], it was shown that a fixed dislocation with an attached inclusion acts as an elastic string returning the inclusion to its equilibrium position where the dislocation length is minimal. This is illustrated schematically in
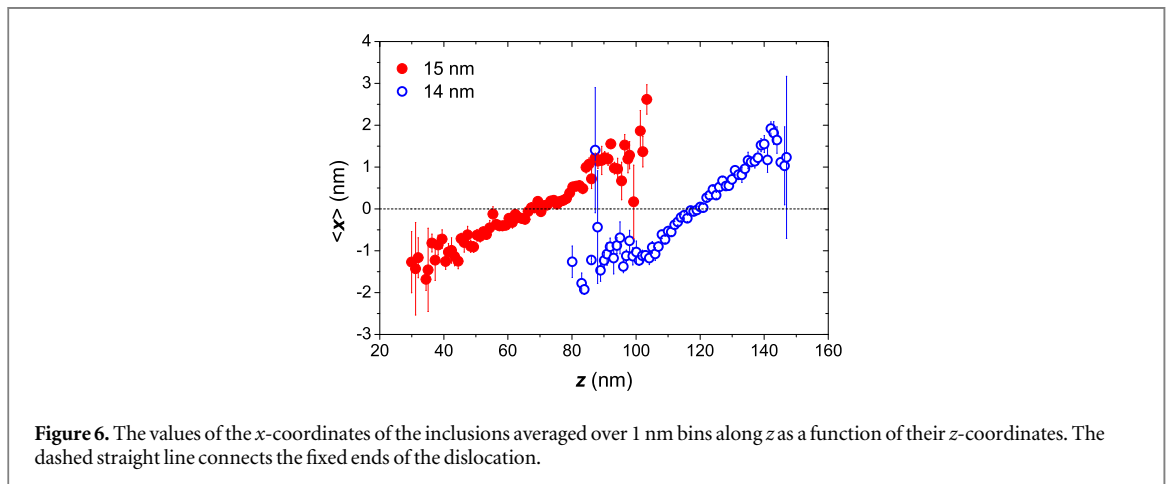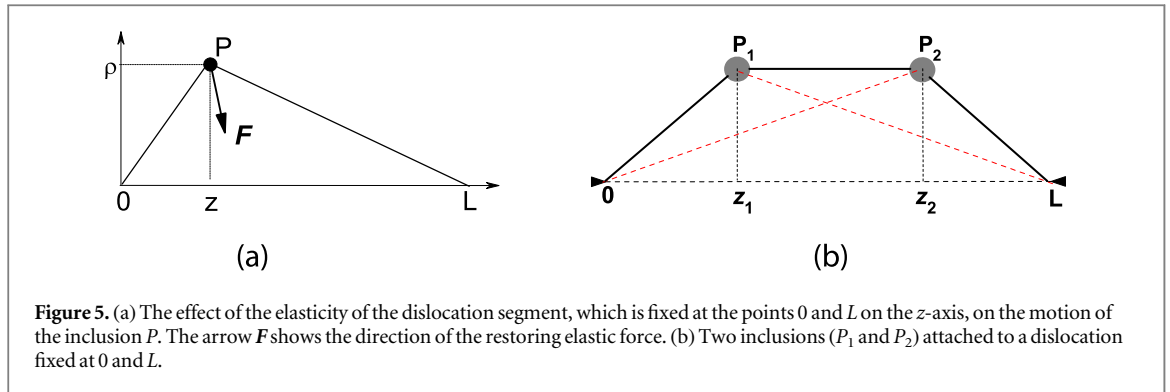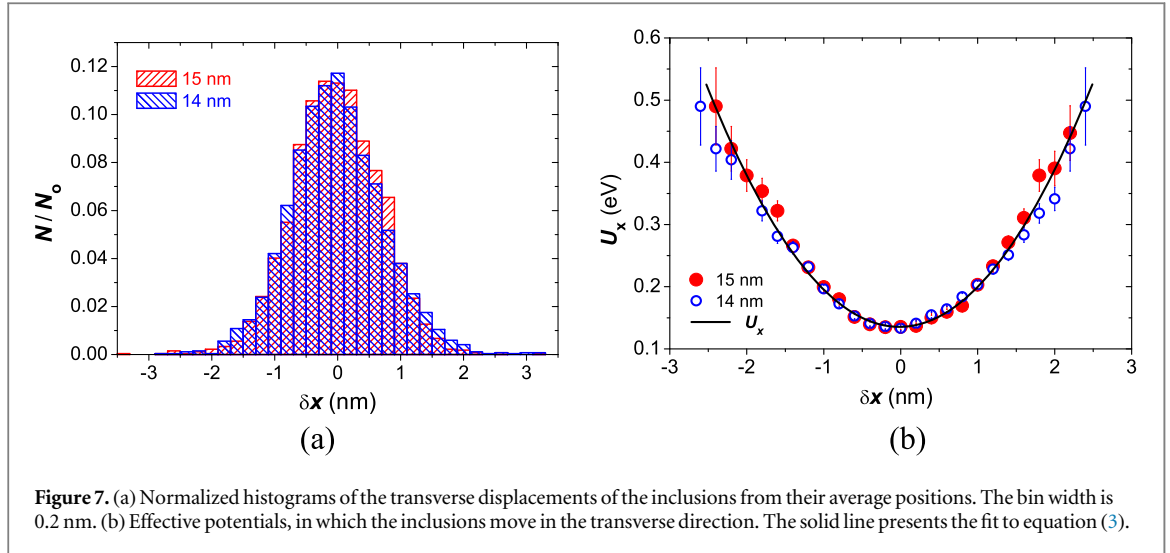
Figure 5. (a) The effect of the elasticity of the dislocation segment, which is fixed at the points 0 and *L* on the *z*-axis, on the motion of the inclusion *P*. The arrow *F* shows the direction of the restoring elastic force. (b) Two inclusions (P_1 and P_2) attached to a dislocation fixed at 0 and *L*.

Figure 6. The values of the *x*-coordinates of the inclusions averaged over 1 nm bins along *z* as a function of their *z*-coordinates. The dashed straight line connects the fixed ends of the dislocation.

figure 5(a) showing the dislocation segment 0*L* with an attached inclusion *P*, that due to its thermal motion is displaced to a point (ρ, z). The arrow in figure 1 shows the restoring force *F* due to the line tension of the dislocation. The projection of *F* on the *Z*-axis is always directed from nearest fixed end of the dislocation, and that is the reason for the random oscillations of the inclusion along the dislocation line. The projection of *F* on the plane perpendicular to the dislocation line causes random transverse oscillations of the inclusion in the vicinity of the equilibrium position of the dislocation.

Figure 5(b) shows schematically a fixed dislocation *OL* with two attached inclusions (P_1 and P_2). The dislocation between them is always stretched due to its line tension as its mobility is much higher, and its inertia is much lower than those of the inclusions. Then, we can consider thermal motion of the inclusions P_1 and P_2 along fixed segments OP_2 and P_1L, respectively, see figure 5(b), as it was done in [3, 5] for a single inclusion on a fixed dislocation. This explains the appearance of the potential wells, in which the inclusions move, and the interaction of the inclusions. Indeed, oscillations of each inclusion lead to random oscillatory shifts of the potential well. Spontaneously, shifts of each potential well will contribute to the motion of its associated inclusion. Then, these inclusions can be considered as random oscillators coupled to some degree. Thus, the interaction of the inclusions is expected to introduce a spatial correlation to their steady state thermal motion.

5. Transverse thermal motion of the inclusions

Figure 6 shows the averaged trajectories of the inclusions attached to the dislocation. To obtain them the dislocation segment was divided into 1 nm intervals. The average value, $\langle x \rangle$ of the *x*-coordinates of points of the trajectories of the inclusions in each of the intervals was found. One can see that the averaged positions of the inclusions form two approximately straight lines, which are nearly parallel and inclined to the dashed straight line connecting the fixed ends of the dislocation. Since the inclusions are attached to the dislocation, their averaged positions depict the average position of the dislocation. The observed inclination of the averaged positions of the inclusions from the dashed straight line is presumably due to an anisotropy of the dislocation energy.

Since the extent of the transverse displacements of the inclusions from the dislocation line characterize the dislocation elasticity [5], then, for each of the intervals of *z* the transverse displacements of the inclusions from

Figure 7. (a) Normalized histograms of the transverse displacements of the inclusions from their average positions. The bin width is 0.2 nm. (b) Effective potentials, in which the inclusions move in the transverse direction. The solid line presents the fit to equation (3).

their average position $\langle x \rangle$, i.e. $\delta x = x - \langle x \rangle$, were determined for all points lying in a given interval. The normalized histograms of δx for the inclusions are shown in figure 7(a). Using the Boltzmann distribution law the effective potentials, in which the inclusions move in the transverse direction, were derived from these histograms, figure 7(b). Both potentials are fitted fairly well to the same parabolic dependence

$$U_X = \frac{f_d \delta x^2}{2} + U_o \tag{3}$$

with the effective force constant $f_d = (12.4 \pm 0.3) \times 10^{-2}$ eV nm^{-2} and $U_o = 0.135 \pm 0.001$ eV, which is introduced because of the uncertainty in the energy level. We note that the theoretical consideration of a single inclusion attached to a fixed dislocation [5] also leads to a parabolic effective potential of its transverse oscillatory motion. However, as the transverse motions of the inclusions are correlated (see next section), the measured δx values are somewhat overestimated as transverse displacements of each of the inclusions contribute to the measured transverse displacement δx of the other inclusion as each of the inclusions is the end of dislocation segment for other inclusion, see figure 5(b), meaning that the value of f_d is underestimated.

6. Spatial correlations in thermal motion of the inclusions

Pearson's correlation coefficients for the z-coordinates of the inclusions, the x-coordinates of the inclusions, and the δx-deviations of the inclusions from the average position of the dislocation, R_z, R_x and $R_{\delta x}$, respectively, were determined using the trajectory points of the inclusions within 2 nm intervals of Δz. The value of R_z in the ith interval of Δz is determined using the equation

$$R_z = \frac{\sum\limits_{n=1}^{N_i}(z_{1n} - \overline{z_1})(z_{2n} - \overline{z_2})}{\left[\sum\limits_{n=1}^{N_i}(z_{1n} - \overline{z_1})^2 \sum\limits_{n=1}^{N_i}(z_{2n} - \overline{z_2})^2\right]^{1/2}}, \tag{4}$$

where $\overline{z_1}$ and $\overline{z_2}$ are the means of the z-coordinates of all points (centers of weight) of the trajectories of the inclusions, and N_i is the number of the data-points in the ith interval of Δz. (The equations for R_x and $R_{\delta x}$ are similar.)

The dependences of R_z, R_x and $R_{\delta X}$ on the longitudinal separation of the inclusions Δz are shown in figure 8. The correlation coefficient R_z depends strongly on the separation of the inclusions, that is it depends on their interaction potential U_{int}, solid line in figure 8(a). The coefficient is close to unity indicating full correlation near the minimum of the potential, while anti-correlation is observed at the edges of U_{int}. The correlation coefficient R_x exhibits a qualitatively similar behavior, figure 8(b). The correlation coefficient $R_{\delta x}$ shows a pronounced trend to decrease as Δz increases, figure 8(c). The effect of the interaction potential is not seen here. Possibly, this dependence has features masked by scatter and large errors of the data-points. One can see that most data-points in the graphs of figure 8 lie outside of the range, where the probability of existence of linear (anti)correlation is less than 95%.

In figure 9(a) $\langle \Delta z_{e1} \rangle = \langle z_1 \rangle - z_o$ and $\langle \Delta z_{e2} \rangle = z_L - \langle z_2 \rangle$ are, respectively, the average distances of the 15 and 14 nm inclusions from the adjacent fixed ends of the dislocation. Here, $\langle z_1 \rangle$ and $\langle z_2 \rangle$ are the average z-
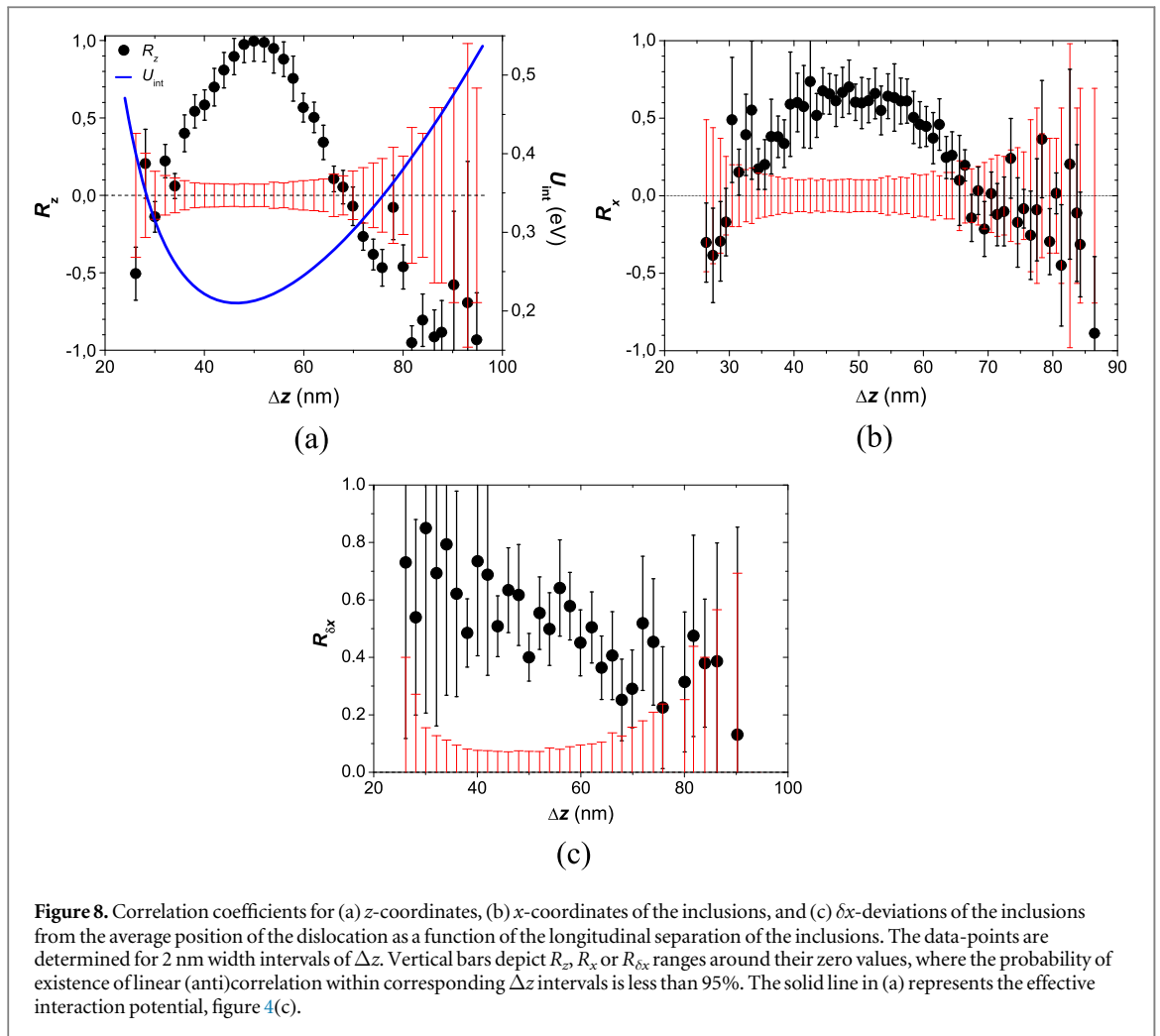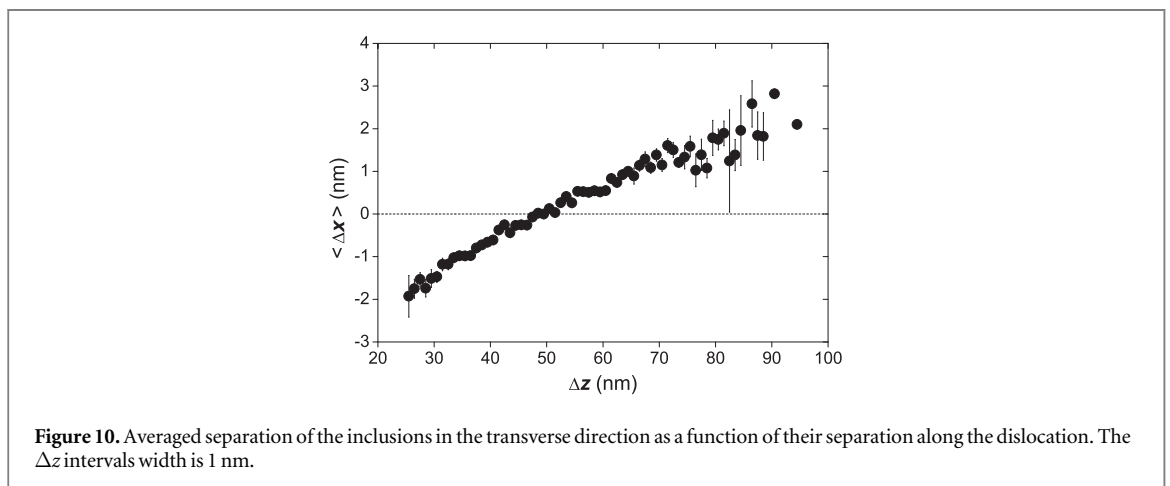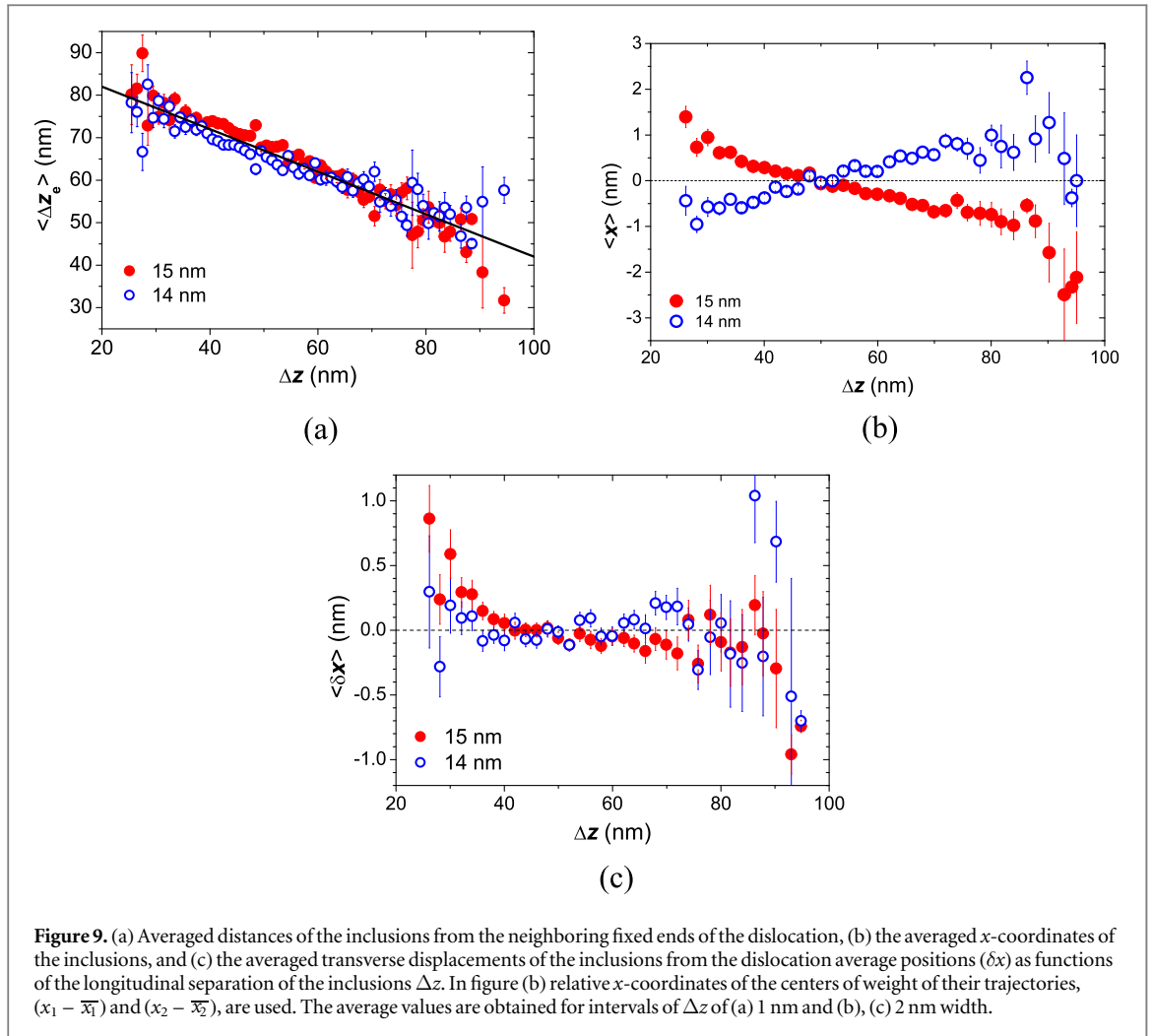
Figure 8. Correlation coefficients for (a) *z*-coordinates, (b) *x*-coordinates of the inclusions, and (c) δx-deviations of the inclusions from the average position of the dislocation as a function of the longitudinal separation of the inclusions. The data-points are determined for 2 nm width intervals of Δz. Vertical bars depict R_z, R_x or $R_{\delta x}$ ranges around their zero values, where the probability of existence of linear (anti)correlation within corresponding Δz intervals is less than 95%. The solid line in (a) represents the effective interaction potential, figure 4(c).

coordinates of the trajectory points of the inclusions within 1 nm intervals of Δz. Remember that $z_o = 0$ and $z_L = L$, then, $\langle \Delta z_{e1} \rangle = \langle z_1 \rangle$ and $\langle \Delta z_{e2} \rangle = L - \langle z_2 \rangle$. The dependence of $\langle \Delta z_{e1} \rangle$ and $\langle \Delta z_{e2} \rangle$ as functions of the inter-inclusion longitudinal separation Δz indicates a correlation between z_1 and z_2. Furthermore, they show that the averaged behavior of the system is very close to being symmetrical around the middle of the dislocation, $\langle \Delta z_{e1} \rangle = \langle \Delta z_{e2} \rangle = \frac{1}{2}(L - \Delta z)$, as shown by the solid straight line in figure 9(a).

The similar dependences of the *x*-coordinates of the inclusions averaged over 2 nm intervals of Δz, $\langle x_1 \rangle$ and $\langle x_2 \rangle$, are shown in figure 9(b). In this figure *x*-coordinates of the centers of weight of the trajectories of the inclusions, $\overline{x_1}$ and $\overline{x_2}$, are taken as zeros. These approximately linear dependences demonstrate strong correlation of x_1 and x_2 with Δz. They suggest also a strong correlation between the *x*-coordinates of the inclusions. Actually, the relative (mutual) arrangement of these dependences is similar to that of the dependences of $\langle z \rangle$ on Δz which can be seen by comparing figures 9(a) and (b). The dependences of the averaged transverse displacements $\langle \delta x \rangle$ of the inclusions on Δz display similar behaviors as well, figure 9(c). So, the correlation of δx-displacements of the inclusions is expected. Here, the width of the Δz intervals is 2 nm. The scattering of the data-points near the ends of the Δz-range in figure 9 is likely due to poor statistics or/and a weaker correlation.

Also, the near-linear dependence of the averaged separation of the inclusions in the transverse direction $\langle \Delta x \rangle = \langle x_2 - x_1 \rangle$ on their separation along the dislocation Δz shown in figure 10 indicates on strong correlation between Δx and Δz.

Plotting the *z*-coordinate for one inclusion as a function of the *z*-coordinate of the other and vice versa (figure 11(a)) displays a similar behavior that is approximately linear. In this figure the *z*-coordinates of the centers of weight of the trajectories of the inclusions, $\overline{z_1}$ and $\overline{z_2}$, are taken as zeros. Similar plots for the *x*-coordinates of the inclusions shown in figure 11(b) demonstrate mutual similar correspondence between $\langle x_1 \rangle$ and $\langle x_2 \rangle$ also. Thus, the dependences in figure 11(a) and in figure 11(b) show a strong spatial correspondence of the averaged positions of the inclusions relative to the centers of weight of their trajectories. This denotes that their chaotic oscillations along the averaged trajectories shown in figure 6 on average are approximately synchronous. Furthermore, figure 11(c) shows the averaged transverse displacements of the inclusions from the

Figure 9. (a) Averaged distances of the inclusions from the neighboring fixed ends of the dislocation, (b) the averaged x-coordinates of the inclusions, and (c) the averaged transverse displacements of the inclusions from the dislocation average positions (δx) as functions of the longitudinal separation of the inclusions Δz. In figure (b) relative x-coordinates of the centers of weight of their trajectories, $(x_1 - \overline{x_1})$ and $(x_2 - \overline{x_2})$, are used. The average values are obtained for intervals of Δz of (a) 1 nm and (b), (c) 2 nm width.

Figure 10. Averaged separation of the inclusions in the transverse direction as a function of their separation along the dislocation. The Δz intervals width is 1 nm.

average position of the dislocation, δx_1 and δx_2, are also on average approximately synchronous. The scatter of the data-points near the ends of the ranges in figure 10 is likely due to a weaker correlation or/and a worse statistics.

Finally, when the z-coordinate of the center of weight of the inclusions $z_{cw} = (z_1 + z_2)/2$ is located in the middle part of the dislocation the changes in the averaged Δz values are small as if the system of the inclusions is approximating a rigid state, figure 12. The averaged Δz decreases, when the center of weight is close to one of the dislocation ends fixed at the large inclusions that provide a strong repulsive interaction with the nearer inclusion. In other words, the inclusions on average form a dumbbell, which contracts only significantly near the fixed ends of the dislocation.

Figure 11. (a) The z-coordinate of 15 nm inclusion averaged over 2 nm intervals as a function of the z-coordinate of 14 nm inclusion and the similar dependence, where the role of the inclusions is exchanged. (b) The x-coordinate of 15 nm inclusion averaged over 2 nm intervals of x-coordinate of 14 nm inclusion and the similar dependence, where the role of the inclusions is exchanged. The coordinates of the inclusions relative to the centers of weight of their trajectories, $(x_1 - \overline{x_1})$, $(z_1 - \overline{z_1})$ and $(x_2 - \overline{x_2})$, $(z_2 - \overline{z_2})$, are used in (a), (b). (c) The transverse displacement of 15 nm inclusion δx_1 averaged over 0.2 nm intervals of the transverse displacement of 14 nm inclusion δx_2 and the similar dependence, where the role of the inclusions is exchanged.

Figure 12. The longitudinal separation of the inclusions averaged over 2 nm width intervals of z-coordinate of their center of weight, z_{cw}.

7. Conclusions

(1) The thermal behavior of a system of two nano-sized liquid Pb inclusions attached to a fixed dislocation in aluminum is studied *in situ* at 447 °C using TEM. Using time resolved observations, their trajectories are determined and analyzed as a function of time.

(2) Oscillatory motion of the inclusions can be explained in terms of thermal motion in coupled potential wells due to the line tension of the dislocation.

(3) The shapes of the effective potentials in which the inclusions move, and of the effective potential of the interaction between the inclusions are determined.

(4) Interaction between the inclusions mediated by the elastic line properties of the dislocation leads to spatially correlated thermal motion both along the dislocation line and transverse to it. The observed correlations of the positions of the inclusions suggest that they on average move almost synchronously along their averaged trajectories. The inclusions on average form a dumbbell, which contracts only significantly near the fixed ends of the dislocation.

Acknowledgments

ORCID iDs

Sergei I Prokofjev ⓘ https://orcid.org/0000-0002-2899-1817

References

[1] Barnes R S and Mazey D J 1963 *Proc. R. Soc.* A **275** 47
[2] Ono K, Furuno S, Hojou K, Izui K, Kino T, Mizuno K and Ito K 1993 *Defect Diffus. Forum* **95-98** 335
[3] Prokofjev S, Zhilin V, Johnson E, Levinsen M T and Dahmen U 2005 *Defect Diffus. Forum* **237–240** 1072
[4] Johnson E, Levinsen M T, Steenstrup S, Prokofjev S, Zhilin V, Dahmen U and Radetic T 2004 *Phil. Mag.* **84** 2663
[5] Johnson E, Prokofjev S, Zhilin V and Dahmen U 2005 *Z. Metallkd.* **96** 1171
[6] Johnson E, Andersen J S, Levinsen M T, Steenstrup S, Prokofjev S, Zhilin V, Dahmen U, Radetic T and Turner J H 2004 *Mater. Sci. Eng.* A **375–377** 951
[7] Johnson E, Steenstrup S, Levinsen M, Prokofjev S, Zhilin V and Dahmen U 2005 *J. Mater. Sci.* **40** 3115
[8] Prokofjev S I, Johnson E, Zhilin V M and Dahmen U 2006 *Adv. Sci. Technol.* **46** 98
[9] Wright R N and Van Siclen C D 1993 *J. Nucl. Mater.* **206** 87
[10] Prokofjev S I, Zhilin V M, Johnson E and Dahmen U 2007 *Defect Diffus. Forum* **264** 55
[11] Gabrisch H, Kjeldgaard L, Johnson E and Dahmen U 2001 *Acta Mater.* **49** 4259
[12] Johnson E, Andersen H H and Dahmen U 2004 *Microsc. Res. Tech.* **64** 356
[13] Willertz L E and Shewmon P G 1970 *Metall. Trans.* **1** 2217
[14] Nichols F A 1969 *J. Nucl. Mater.* **30** 143
[15] Hirth J P and Lothe J 1982 *Theory of Dislocations* (New York: Wiley)
[16] Nembach E 1996 *Particle Strengthening of Metals and Alloys* (New York: Wiley)
[17] Argon A S 2008 *Strengthening Mechanisms in Crystal Plasticity* (New York: Oxford University Press)
[18] Lücke K and Granato A V 1981 *Phys. Rev.* B **24** 6991
[19] Granato A V and Lücke K 1981 *Phys. Rev.* B **24** 7007
[20] Geguzin Y E and Krivoglaz M A 1973 *Migration of Macroscopic Inclusions in Solids* (New York: Consultants Bureau)
[21] Massalski T B (ed) 1986 *Binary Alloy Phase Diagrams* vol 1 (Metals Park, OH: ASM) p 147